Electrochemical Synthesis of 3D Porous $Co(OH)_2$/ErGO Nanoflake for High-Performance Supercapacitor and Non-Enzymatic Glucose Sensor

ZHANG Qi[1,a], LIU Hui[1,b], ZHANG Cunrong[1,c], GENG Xiujuan[1,d], XU Yongji[1,f]
YANG Yu[1,g]*and WANG Lei[1,h]
[1]Key Laboratory of Eco-chemical Engineering, Ministry of Education,
Inorganic Synthesis and Applied Chemistry, College of Chemistry and Molecular Engineering,
Qingdao University of Science and Technology, Qingdao 266042, P. R. China
[a]506588301@qq.com, [b]296461153@qq.com, [c]1663127627@qq.com, [d]xiujuangeng@foxmail.com
[f]1732013640@qq.com, [g]yangyu9039@163.com, [h]inorchemwl@163.com

Keywords: supercapacitors; graphene; $Co(OH)_2$; glucose sensor

Abstract $Co(OH)_2$ is a promising electrochemical material owing to its high theoretical specific capacitance, low cost and eco-friendliness. However, the poor conductivity hinders its application. In this work, 3D porous $Co(OH)_2$/ErGO nanoflake vertically grown on the surface of Ni foam (NF) through a facile two-step electrodeposition approach, avoiding the need for binders and conducting agents. When used for supercapacitors (SCs), the $Co(OH)_2$/ErGO/NF electrode exhibits a high specific capacitance of 857.1 F g^{-1} at a current density of 2 A g^{-1}, and a favorable cycling stability with 85.0% retention even at 12 A g^{-1} after 2000 cycles. Additionally, serving as a non-enzymatic sensor, the 3D $Co(OH)_2$/ErGO/NF electrode exhibits remarkable electrocatalytic activity towards glucose oxidation with a high sensitivity of 10.2 mA mM^{-1} cm^{-2}. Owing to its favorable electrochemical performance, the 3D $Co(OH)_2$/ErGO/NF electrode with porous structure has great potential applications in the fields of electrochemical SCs and non-enzymatic glucose sensors.

Introduction

Supercapacitors (SCs) are considered as promising candidates for energy storage due to high power density, fast charge and discharge rates and long cycle life [1]. According to the storage mechanisms, SCs can be classified as electroch emical double-layer capacitors and pseudocapacitors [2]. The former is based on non-faradic process in high surface area of carbon material like active carbon, graphene *etc*., and the latter make use of continuous redox action between electrolytes and electrode materials like conducting polymer, metal oxide or LDH *etc*. [3]. Since electrode materials play important role in SC performance, great efforts have been devoted to the synthesis of advanced materials with high specific capacitance.

$Co(OH)_2$ is one of the most promising candidates in high performance SCs owing to its excellent redox activity, low cost and porous nanostructure [4-5]. Up to now, various morphologies of $Co(OH)_2$ have been reported with different methods [4-11]. Reduced GO (rGO) shows higher electric conductivity and specific surface area, can be also used in energy converse device [12-13]. However, the low capacitance and energy density limit the application in SC. To overcome these problems, an alternative method is fabricating graphene-based nanocomposites for high-performance SCs and biosensors [14-15]. 3D $Co(OH)_2$/ErGO electrode materials is attractive because of the potential of composite structure. Such a research direction has been reported [16-17], however, this composite synthesized by electrochemical deposition has not been reported, and little research has so far been carried out on the use of $Co(OH)_2$ for glucose probe [18].

Glucose detection is critical to the diagnosis and management of diabetes. For most glucose sensors, the detection is indirect and mediated by enzymes such as glucose oxidase. The need for enzyme proteins compromises the stability, sensitivity reproducibility, and cost-efficiency of the sensor due to the poor tolerance to non-physiological chemical environments and the sensitivity to temperature, pH, humidity, *etc*. [19]. Recently, it has been demonstrated that metal catalysts are able to catalyse oxidation of glucose and therefore direct electrochemical detection of glucose without the need for any

enzymes could be achieved [20-21]. To our knowledge, nanostructured $Co(OH)_2$ possesses high specific surface, electroactive area and excellent biocompatibility [18], which made it as a promising candidate for glucose probe.

To develop $Co(OH)_2$/ErGO composite electrodes having good rate capability, long cycle stability and high specific capacitance, 3D interconnected $Co(OH)_2$/ErGO composite grown on the NF were fabricated by simple and green electrochemical deposition in this paper. The interconnected structure of $Co(OH)_2$ ensures fast ions diffusion, ErGO electrochemical reduced from GO provides high surface area and good conductivity. The $Co(OH)_2$/ErGO/NF composite electrode shows excellent electrochemical capacitive properties with high specific capacitance of 857.1 F g^{-1} at a current density of 2 A g^{-1}, good rate capability and long-term cycling stability. Serving as a non-enzymatic glucose sensor, the 3D $Co(OH)_2$/ErGO/NF electrode shows a high sensitivity of 10.2 mA mM^{-1} cm^{-2} for glucose. All these impressive results indicate that $Co(OH)_2$/ErGO is quite promising for applications in SCs and non-enzymatic glucose sensors.

Experimental

Synthesis of ErGO on NF.GO was synthesized from graphite powder by the modified Hummers' method [22]. 20 mg GO was mixed with 20 mL PBS solution (pH 8.0) and ultrasonicated for 2 h to yield a stable GO suspension (1 mg mL^{-1}). Typically, the ErGO electrode was fabricated by electrochemical reduction of GO suspension on a piece of NF under a constant potential of -1.2 V (vs.SCE) for 600 s.

Preparation of 3D porous $Co(OH)_2$ nanoflake film on ErGO/NF. The electrodeposition was performed in a standard three-electrode glass cell at 25 °C, with the ErGO/NF as the working electrode, a saturated calomel electrode (SCE) as the reference electrode, and a platinum plate as the counter electrode. 3D porous $Co(OH)_2$ nanoflake was electrodeposited in an aqueous solution containing 0.1 M $Co(NO_3)_2$ with potential at -0.9 V for 300 s. The electrodeposition process of the $Co(OH)_2$ nanoflake expressed as follows [23]:

$$NO_3^- + 7H_2O + 8e^- \rightarrow NH_4^+ + 10OH^- \quad (1)$$

$$Co^{2+} + 2OH^- \rightarrow Co(OH)_2 \quad (2)$$

After deposition, the 3D $Co(OH)_2$/ErGO/NF electrode was rinsed with distilled water and dried in a vacuum oven at 40 °C for 12 h. The load weight of $Co(OH)_2$ and ErGO was approximately 2.0 mg cm^{-2} by weighing the electrode before and after electrodeposition.

Results and discussion

Structure and morphology characterization. Morphologies of the as-prepared ErGO/NF and $Co(OH)_2$/ErGO/NF were characterized by SEM. Fig. 1a shows the typical surface morphology of ErGO/NF with a unique 3D interconnected structure which belongs to NF. Fig. 1b shows obvious wrinkles on the surface of NF, which indicated the existence of ErGO. The wrinkle structure highly increased the specific surface area, which can provide enough space for active materials; on the other hand, the ErGO can also improve the electrical conductivity of materials. SEM images of 3D $Co(OH)_2$/ErGO/NF are shown in Fig. 1c and d, many nanoflakes grow vertically and cross-link on the framework of ErGO/NF, forming a three dimensional structure with obvious pores. The porous nanostructure of $Co(OH)_2$ can provide a high specific surface area that can support more active sites; in addition, the existence of pore provide path for electrolyte ions and electronics, which increase the diffusion rate and lead to high power. Therefore, this structure may contributes to the high specific capacitance and high power density of this electrode material.

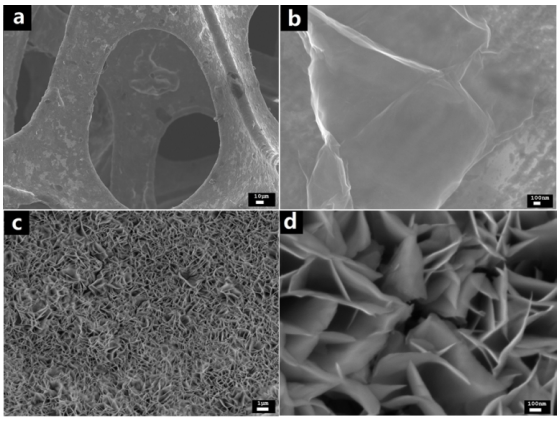

Figure 1 SEM images for ErGO/NF (a,b) and 3D $Co(OH)_2$/ErGO/NF (c,d)

The Raman spectra of GO and ErGO was further recorded and shown in Fig. 2a. Both of the spectra of GO and ErGO display the existence of characteristic peaks: D and G bands, which located at 1352 and 1585 cm^{-1}. The intensity ratio (I_D/I_G) of D and G bands is 0.97 in GO and increases to 1.06 in ErGO, demonstrating that the chemical reduction alters the structure of GO and introduces a large number of structural defects. Fig. 2b shows the XRD pattern for 3D $Co(OH)_2$/ErGO/NF, wherein the peaks at 2θ values of 19.6˚, 34.9˚, 41.3˚, 53.2˚ and 57.6˚ are respectively indexed to $Co(OH)_2$ (001), (100), (101), (102), (110) (PDF, card no. 30-0443). The peaks at 44.6˚, 51.89˚and 76.5˚ are from NF (PDF, card no. 04-0850). No obvious diffraction peak of graphene was observed, which may be due to strong peaks from NF overlapped the signal of the graphene. Energy-dispersive X-ray spectrometer (EDS) in Fig. 2c confirms the presence of the elements of cobalt, oxygen, carbon and nickel in the deposited materials, whereas no other chemical elements exist.

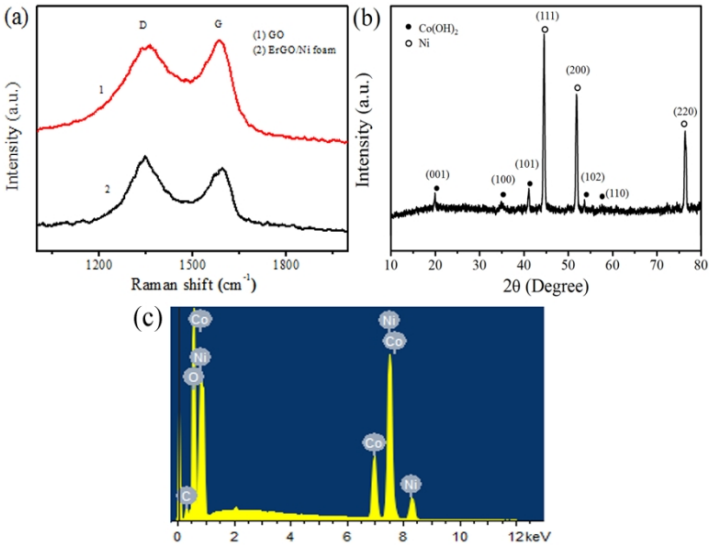

Figure 2 Raman spectra of GO, ErGO (a), XRD pattern (b) and EDS spectra (c) of 3D $Co(OH)_2$/ErGO/NF

Considering these above results, it is justified that a 3D porous $Co(OH)_2$/ErGO nanoflake has been successfully constructed on NF via two-step electrodeposition methods. As shown in Scheme 1, firstly, ErGO nanofilms were directly grown on the NF by electrodeposition. Secondly, $Co(OH)_2$ nanoflake were vertically growing on the surface of ErGO/NF by successive electrodepositon. The nanoflakes cross-link on the framework of ErGO/NF to form 3D net structure with obvious pores, which can support high ions diffusion rate and more active sites. In addition, no binder existed among $Co(OH)_2$, ErGO and NF, which can afford an effective electron transport pathway.

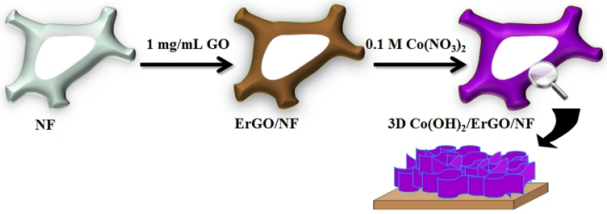

Scheme 1. Schematic illustration for the formation of 3D $Co(OH)_2$/ErGO/NF electrode

Electrochemical capacitive properties for SC. Figure 3a presents the Cyclic voltammograms (CV) curves of the 3D $Co(OH)_2$/ErGO/NF and ErGO/NF with a potential window of -0.2 to 0.5 V at 10 mV s^{-1}. The CV curve of ErGO/NF electrode exhibits a pair of weak redox peaks because the reversible reactions of Ni(II)/Ni(III) formed on the NF surface in the alkaline electrolyte. When $Co(OH)_2$ was introduced to ErGO/NF, a pair of strong peaks were observed, implying the presence of a reversible faradaic reaction and pseudocapacitive behavior, and the redox reaction: $Co(OH)_2 + OH^- \rightarrow CoOOH + H_2O + e^-$ occurs near the surface of electrode material and lead to much greater charge storage than EDLCs. Therefore, the 3D $Co(OH)_2$/ErGO/NF electrode has a large capacitance and the contribution of NF to the total electrochemical capacitance can be negligible for the electrode.

The CV curves of 3D $Co(OH)_2$/ErGO/NF at different scan rates (2, 5, 10, 25 and 40 mV s^{-1}) are shown in Figure 3b. The CV curves keep the same shape with increasing the scan rate, suggesting a good rate capability and reversibility. This result can be attributed to the porous structure of $Co(OH)_2$ and the conductive ErGO. Figure 3c displays a set of galvanostatic discharge curves with increasing current densities from 2 to 16 A g^{-1}, the observed nonlinear curves indicate the pseudocapacitance nature, which is consistent with the CV curves. The specific capacitance can be calculated according to the following equation:

$$C = (I \cdot \Delta t)/(m \cdot \Delta V) \quad (1)$$

Where C_m (F g^{-1}) is the specific capacitance, I (mA) is the charge/discharge current, Δt (s) is the discharge time, ΔV (V) represents the potential window, and m (mg) is the mass of the $Co(OH)_2$ and ErGO within the electrode.

The specific capacitance is calculated to be about 857.1, 811.6, 783.3, 664.7 and 657.5 F g^{-1} at the current densities of 2, 4, 6, 8, and 16 A g^{-1}, respectively. This observed specific capacitance is comparable with other reported $Co(OH)_2$ nanomaterials as shown in Tab. 1, which demonstrates the obtained 3D porous $Co(OH)_2$/ErGO/NF electrode possesses a high specific capacitance. The electrode still reserved 76.7% of the specific capacitance in 2 A g^{-1} with the current density increasing to 16 A g^{-1} indicating the high rate capability.

Table 1 Summary of capacitive performance of reported $Co(OH)_2$ with different morphologies

electrode material	Specific capacitance	Cycling stability	Ref.
Flower-like $Co(OH)_2$	429 F g^{-1} (1 A g^{-1})	-	11
$Co(OH)_2$ nanowires	1180 F g-1 (4 A g-1)	1000 cycles (< 52%)	7
β-$Co(OH)_2$	416 F g^{-1} (1 A g^{-1})	500 cycles (> 93%)	9
$Co(OH)_2$ nanoflakes	559.15 F g^{-1} (10 mA cm^{-2})	1000 cycles (> 87%)	10
$Co(OH)_2$/GO	474 F g^{-1} (1 A g^{-1})	1000 cycles (> 90%)	5
$Co(OH)_2$/ErGO	857.1 F g^{-1} (2 A g^{-1})	2000 cycles (> 85%)	Our work

Fig. 3d shows the Nyquist plots of the ErGO/NF, 3D $Co(OH)_2$/ErGO/NF and $Co(OH)_2$/NF electrodes in the frequency range from 0.01 to 10^5 Hz. The 3D $Co(OH)_2$/ErGO/NF electrode shows only slightly larger charge transfer resistance (*R*ct) compared with the ErGO/NF electrode, implying excellent electrical conductivity for this composite electrode. The *R*ct increases in the absence of ErGO, indicating that ErGO in the composite will take the price of low electrical conductivity. In the high frequency region, the intercept at real part (Z') represents the equivalent series resistance (ESR), the values of ErGO/NF and 3D $Co(OH)_2$/ErGO/NF electrode are 2.07 and 2.12, respectively. The nearly equal value indicating the excellent contact between $Co(OH)_2$ and ErGO sheet. Fig. 3e shows the first ten charge-discharge curves of the 3D $Co(OH)_2$/ErGO/NF between 0 to 0.45 V at 12 A g^{-1}. All the GCD curves are nearly symmetric in shape, indicating good electrochemical reversibility and good capacitive behavior. The cycling response up to 2000 cycles is shown in Fig. 3f, 85.0% of the initial specific capacitance remains at 12 A g^{-1}, indicating the high cycle stability.

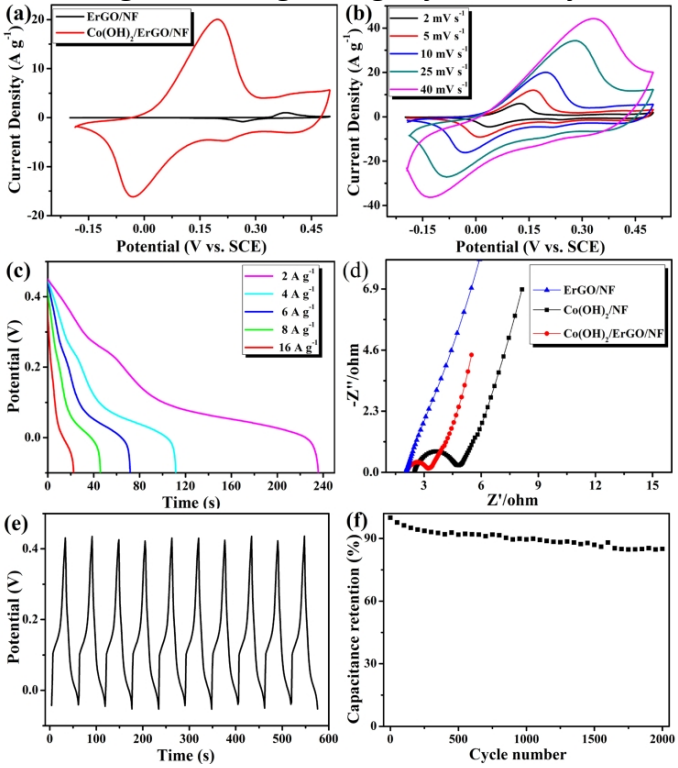

Figure 3 Electrochemical properties of $Co(OH)_2$/ErGO/NF electrodes measured using a three-electrode system in 1.0 M KOH solution. (a) the comparative CV curves of 3D $Co(OH)_2$/ErGO and ErGO on NF at 10 mV s^{-1}. (b) CVs of 3D $Co(OH)_2$/ErGO/NF electrode at different scan rates. (c) discharge curves of $Co(OH)_2$/ErGO/NF electrode at different current densities. (d) Nyquist plots for the $Co(OH)_2$/NF, ErGO/NF and 3D $Co(OH)_2$/ErGO/NF electrodes. (e) the first ten GCD curves and(f) cycling performance of $Co(OH)_2$/ErGO/NF at 12 A g^{-1}.

$Co(OH)_2$/ErGO/NF electrode for non-enzymatic glucose detection. The 3D $Co(OH)_2$/ErGO/NF has been further explored to detect glucose in 0.5 M NaOH. Fig. 4a shows the CV curves of the electrode at different scan rates in 0.5 M NaOH solution. The shape of CV curves didn't change with the increasing scan rate, indicating the good rate capability in NaOH electrolyte. Fig. 4b displays the CV curves of the electrode in 0.5 M NaOH with different concentration of glucose from 0 to 1 mM at a scan rate of 10 mV s^{-1}. With the addition of glucose, peak current at about 0.4 V was growing. Fig. 4c shows the typical amperometric responses of the 3D $Co(OH)_2$/ErGO/NF electrode to successive addition of glucose into NaOH solution. A steep increase in current responses is obtained, indicating that 3D $Co(OH)_2$/ErGO/NF exhibits very sensitive and rapid response. The inset shows the obvious amperometric response of the electrode toward the addition of 0.1 μM glucose with a signal-to-noise ratio (S/N) of ~ 5. As shown in Fig. 4d, a linear relationship (R^2 = 0.9983) was observed over the range of 0.1 ~ 150 μM. The linear regression equation was I = 23.96 + 10.20$C_{glucose}$(mM), which indicated the extraordinary sensitivity of 10.2 mA mM^{-1} cm^{-2} is obtained.

Selectivity is another major characteristic of high-performance non-enzymatic glucose sensors. The effects of common interfering species such as ascorbic acid, uric acid, L-Cys, Lactose and Salic which may be present in human body serum are investigated. In normal human body, the concentration of glucose in serum is about 3 ~ 8 mM, while the interfering species is less than 0.1 mM [24]. For this reason, 1 mM glucose and 0.05 mM other disturbing components was used in the chronoamperometry experiments. Fig. 4e shows the amperometric responses of the electrod with successive addition of 1 mM glucose, 0.05 mM Lactose, L-Cys, AA, UA, and Salic. The addition of 1 mM glucose increased the current signal, which can be attributed to the oxidation of glucose, while no obvious response can be seen in the presence of disturbing components, which suggest this sensor system is feasible for the determination of glucose in the presence of common interfering compounds. Besides, the amperometric response is performed with 0.5 mM glucose in a high chloride ion concentration (0.5 M NaOH + 0.5 M NaCl) in Fig. 4f, which demonstrate that the 3D $Co(OH)_2$/ErGO/NF electrode is also immune to high chloride ion concentration.

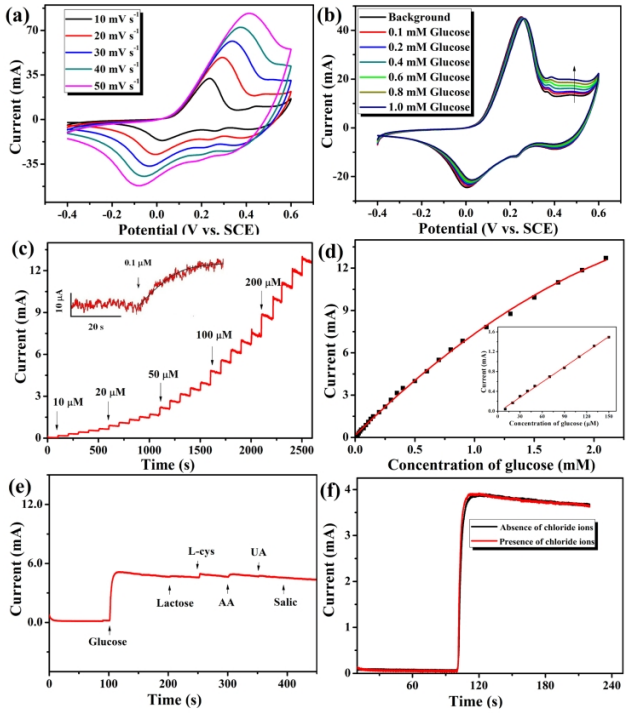

Figure 4 Electrochemical properties of $Co(OH)_2$/ErGO/NF electrodes measured using a three-electrode system in 0.5 M NaOH solution. (a) CV curves measured at 10, 20, 30, 40 and 50 mV s^{-1}. (b) CV curves in the presence glucose at 20 mV s^{-1}. (c) amperometric response of the composite electrode (holding at 0.4 V) with successive addition of glucose in NaOH solution (The inset: amperoetric response to the addition of 0.1 μM glucose). (d) the corresponding calibration curve with a linear fitting at lower concentration range (the inset) (e) the current responses of the electrode to the successive addition of 1 mM glucose, 0.05 mM Lactose, L-Cys, AA, UA, and Salic. (f) the current response to the addition of 0.5 mM glucose with and without 0.5 M NaCl.

Conclusions

In summary, a facile two-step electrodeposition method is employed to synthesize 3D porous $Co(OH)_2$/ErGO nanoflake film on NF. The as-prepared 3D porous $Co(OH)_2$/ErGO/NF electrode provides fast ion and electron transport, a large electroactive surface area, and excellent structural stability. As a result, this porous material exhibits superior pseudocapacitive performance with a high specific capacitance, good rate capability and excellent cycling stability. Moreover, the 3D $Co(OH)_2$/ErGO/NF electrode exhibits remarkable electrocatalytic activity towards glucose with high sensitivity, good selectivity and a rapid response. In a word, the 3D $Co(OH)_2$/ErGO/NF fabricated by

simple electrodeposition is a promising electrode material in SC application and non-enzymatic glucose detection.

Acknowledgements

The authors would like to thank the National Natural Science Foundation of China (Nos: 51571112, 51572136); Natural Science Foundation of Shandong Provincial (ZR2016EMP02); the Natural Science Foundation of Qingdao (16-5-1-83-jch).

References

[1] B. E. Conway: *Electrochemical Supercapacitors: Scientific Fundamentals and Technological Applications* (Kluwer Academic/Plenum, New York 1999)
[2] P. Simon, Y. Gogotsi: Nat. Mater Vol. 7 (2008), p. 845
[3] R. Oraon, A. De Adhikari, S.K. Tiwari and G. C. Nayak: DOI: 10.1039/c6dt00600k
[4] L. Wang, Z.H. Dong, Z.G. Wang, F.X. Zhang and J. Jin: Adv. Funct. Mater. Vol. 23 (2013), p. 2758
[5] S. Chen, J. Zhu, X. Wang, J. Phys. Chem. C Vol. 114 (2010), p. 11829
[6] Z. Li, J. Wang, L. Niu, J. Sun, P. Gong, W. Hong, L. Ma and S. Yang: J. Power Sources Vol. 245 (2014), p. 224
[7] T. Xue and J.M. Lee: J. Power Sources Vol. 245 (2014), p. 194;(c) H.B. Li, M.H. Yu, X.H. Lu, P. Liu, Y. Liang, J. Xiao, Y.X. Tong and G.W. Yang: ACS Appl. Mater. Interfaces Vol. 6 (2014), p. 745; (d) J.K. Chang, C.M. Wu and I.W. Sun: J. Mater. Chem. Vol. 20 (2010), p. 3729
[8] B.G. Choi, M. Yang, S.C. Jung, K.G. Lee, J.G. Kim, H. Park, T.J. Park, S.B. Lee, Y.K. Han and Y.S. Huh: ACS Nano Vol. 7 (2013), p. 2453
[9] C. Mondal, M. Ganguly, P.K. Manna, S.M. Yusuf and T. Pal: Langmuir Vol. 29 (2013), p. 9179
[10] M. Li, S. Xu, T. Liu, F. Wang, P. Yang, L. Wang and P.K. Chub: J. Mater. Chem. A Vol. 1 (2012), p. 532
[11] R. Wang, X. Yan, J. Lang, Z. Zheng and P. Zhang: J. Mater. Chem. A Vol: 2 (2014), p. 12724
[12] (a) C. Ogata, R. Kurogi, K. Hatakeyama, T. Taniguchi, M. Koinuma, and Y. Matsumoto: Chem. Commun Vol. 52 (2016), Vol. 3919
[13] R. Raccichini, A. Varzi, S. Passerini and B. Scrosati: Nat. Mater. Vol. 14 (2015), p. 271
[14] J. Yan, Z. Fan, T. Wei, W. Qian, M. Zhang and F. Wei: Carbon Vol. 48 (2010), p. 3825;
[15] S. Guo and S. Dong: Chem. Soc. Rev. Vol. 40 (2011), p. 2644
[16] J. Xu, K. Wang, S. Z. Zu, B. H. Han and Z.Wei: ACS nano Vol. 4 (2010), p. 5019
[17] D. Wu, F. Zhang, H. Liang and X. Feng: Chem. Soc. Rev. Vol. 41(2012), p. 6160
[18] U.M. Patil, S.C. Lee, J.S. Sohn, S.B. Kulkarni, K.V. Gurav, J.H. Kim, S. Lee and S.C. Jun: Electrochim. Acta Vol. 129 (2014), p. 334
[19] Z. Zhu, L. Garcia-Gancedo, A.J. Flewitt, H. Xie, F. Moussy and W.I. Milne: Sensors Vol.12 (2012), p. 5996
[20] W. Lu, X. Qin, A.M. Asiri, A.O. AlYoubi and X. Sun: Analyst Vol. 138 (2013), p. 417
[21] M. Ma, Z. Miao, D. Zhang, X. Du, Y. Zhang, C. Zhang, J. Lin and Q. Chen: Biosens. Bioelectron. Vol. 64 (2015), p. 477
[22] W. S. Hummers and R. E. Offeman: J. Am. Chem. Soc Vol. 80 (1958), p. 1339
[23] R.B. Rakhi, W. Chen, M.N. Hedhili, D. Cha and H.N. Alshareef: ACS Appl. Mater. Interfaces Vol. 6 (2014), p. 4196
[24] C. Guo, Y. Wang, Y. Zhao and C. Xu: Anal. Methods Vol. 5 (2013), p. 1644